

FULL-SCALE URANS PREDICTION OF A VESSEL'S TRANSVERSE STABILITY IN WIND AND WAVES UNDER LIFTING CONDITION

Reference NO. IJME 811, DOI: 10.5750/ijme.v164iA2.811

Y Yu¹, Australian Maritime College, UTas, Australia, Z Kok, AMC search Ltd., UTas, Australia, S Chai, Australian Maritime College, H Enshaei, Australian Maritime College, M Woodward, Australian Maritime College.

KEY DATES: Submitted: 22/11/21; Final acceptance: 05/10/22; Published: 30/11/22

SUMMARY

Predicting a vessel's motion response is important for the design as well as evaluating its operability and sustainability. This is often performed in towing tanks through captive model test. However, discrepancies exist between model-scale and full-scale results. Besides, quite often, the wind is not included in the test, resulting in unrealistic assumptions of static pressure and constant heeling lever from the wind. This paper presents a study on transverse stability under wind, waves, and lifting conditions, incorporating several series of URANS-based (Unsteady Reynolds-averaged Navier-Stokes) simulations in model scale and full scale. According to the results, scaling effect accounts for about 3~15% in terms of roll amplitude and it seems to be both frictional-force-related and wave-frequency-dependent. In calm water, wind force exerts limited influence on the vessel's transverse stability. However, in regular beam waves especially in longer waves, a wind of 25 m/s increases the roll amplitude up to 53% and the extent of its influence appears to be wave frequency-dependant. The correlation between roll motion and wind/waves/lifting is complicated but their combination produces way more influence than any individual factor alone, indicating none of them should be neglected.

KEYWORDS

URANS, full-scale CFD, wind effects, lifting condition, beam seas

NOMENCLATURE

		P	Pressure (N m ⁻²)
		PF	Potential Flow
B	Moulded breadth (m)	Pos.	Position of the suspended load
CFD	Computational Fluid Dynamics	q_A	Dynamic air pressure
CFL	Courant-Friedrichs-Lewy		
CoG	Centre of Gravity	R	Ratio of convergence
C_{DAY}	aerodynamic force coefficient	R_{AAY}	Aerodynamic force at Y direction
D	Moulded depth – The vertical distance measured amidship from the top of the keel to the top of the freeboard deck beam at side	RAO	Roll Amplitude Operator
		S	Numerical solution
		t	time (s)
DoF	Degree of freedom	TCG	Transverse Centre of Gravity
EFD	Experimental Fluid Dynamics	TF ₄₄	Transfer function for roll motion
f	Wave frequency (Hz)	URANS	Unsteady Reynolds-averaged Navier-Stokes
f_0	Roll natural frequency (Hz)	u	Fluid velocity (m/s)
GM	Metacentric height (m)	U	Numerical uncertainty
H_w	Wave height (m)	V_{AY}	Height-averaged wind speed at transverse (Y) direction (m/s)
H_L	Mean height in lateral plane (m)	V_Z	Height-averaged wind speed at vertical (Z) direction (m/s)
IMO	International Maritime Organisation	v_S	Travel speed of the fluid element
IS	Intact Stability	W_{Lift}	Weight of the lifted object
ITTC	International Towing Tank Conference	x	Distance that the fluid element travels (m)
k	Wave number	z	vertical direction (Z-axis)
LC	Loading Condition	ρ	Density of water (kg m ⁻³)
Loa	Length overall (m)	g	Gravitational acceleration
Lpp	Length between perpendiculars (m)		
MSC	Maritime Safety Committee		

¹ Corresponding author, Australia Maritime College, University of Tasmania, Australia

Email address: yaru.yu@utas.edu.au, <https://orcid.org/0000-0002-2347-4669>, F08 Connell building (AMC, UTAS), Locked Bag 1399, 100 Maritime Way, Newnham, Launceston, TAS, 7248, Australia

μ	Dynamic viscosity
π	The ratio of a circle's circumference to its diameter (3.14)
D	Mass displacement (tonnes)
ϑ	Wave slope
φ	Roll amplitude
Δl	length of mesh cell (m)
τ_{ij}	Mean viscous stress tensor

1. INTRODUCTION

Motion prediction of a sea-going vessel is important from the perspectives of both design and operation. Traditional approaches involve potential flow theory in frequency domain with the assumption that the curl of the gradient of a scalar always being zero. Over the years, the application of this theory has evolved from two-dimensional strip method to three-dimensional panel method. But none of them accounts for viscous effects and flow turbulence. Recent development in terms of Computational Fluid Dynamics (CFD), typically the unsteady Reynolds-Averaged Navier-Stokes (URANS) method tends to be more precise in predicting a ship's hydrodynamics and motion responses. It also offers a realistic virtual environment in which the wind, waves, and particulars of the vessel can be considered in a holistic manner.

Captive scale-model tests, as commonly performed in towing tanks, are often used to predict a ship's motion. When test results are extrapolated to full scale, discrepancies in Reynolds number are introduced since this process is governed by Froude Similarity Law. Concerns are mostly related to the discrepancies in terms of flow features such as boundary layers, wave breaking, and flow separation, which is commonly referred to as scale effects. While scale effects on vessels' resistance are considered by flat plate correlations, its influence on roll motion response is rarely discussed. One of the challenges is the non-linearity of roll motion and roll damping which has not been fully understood (ITTC, 2021a). Since it is difficult to compare the results between scale-model test and full-scale sea trial due to the limited data available, numerical simulations may be a good alternative to study scale effects.

The significance of scale effects is known to vary from study to study. For example, (Kok et al., 2020) compared results between full-scale and model-scale CFD using a validated numerical model and found that scale effects on container squat is insignificant. However, (Jin et al., 2015) carried out a series of URANS-based simulations after validating a numerical set-up with several different scales of models and found that surge and sway forces are affected by scale effect, but yaw moment is not significantly affected. Due to the difference of Reynolds number between full scale and model scale, viscous boundary layers are thinner in full scale and therefore, skin frictions are reduced. Subsequently, the pressure distribution in the boundary layer region around the stern and near wake region is also changed (Oh and Kang, 1992). When

a vessel rolls in waves, skin friction is an important part of the roll damping. Due to the difference of boundary layers between full scale and model scale, roll motion differ and so is the transverse stability of the vessel. This study focuses on transverse stability of a vessel at sea, therefore, it would be worthwhile investigating the influence of scale effects on roll motion to form a basic understanding in this field.

A second consideration of the influential factor on motion prediction is wind load which normally exerts limited influence on marine structures that amount to only a fraction of the total loading. But there are circumstances such as dynamic positioning, lifting operation, and vessels with large windage areas (e.g., cruise vessels, navy ships, containers, etc.) when wind load becomes considerable. In the 2008 Intact Stability Code (IMO, 2008), the criteria refer to predefined wind pressure of 504 Pa and wind effects were discussed as early as 1985 when IMO adopted Resolution A.562(14) (IMO, 1985) as a recommendation. Later on, it was made mandatory by the 2008 IS CODE (IMO, 2008). Although it somewhat accounts for ship roll dynamics, it is still a static approach, calculating wind heeling lever based on a set of simplified assumptions such as constant wind speed and steady wind pressure. As a result, criticism arose (Vassalos et al., 2003, Saydam and Taylan, 2018, Spyrou, 2011). To address these issues, the Maritime Safety Committee (MSC) approved guidelines (MSC.1/Circ.1200) as alternative means (in particular, model experiments) for assessment of the weather criterion, and included them into resolution A.749(18) (IMO, 1993). Following these guidelines, wind effects are studied in wind tunnels and relevant research can be found in (Deakin and Wright, 2005, Janssen et al., 2017, Andersen, 2013). However, wind tunnel tests for marine applications normally fix the model with load cells, which measure the values of wind loads and moments, but few of them include motions prediction; the dynamic effects from the model are not considered. Although the static wind-induced heel angle was calculated during wind tunnel tests in some cases, it can be quite different from those in wind with waves due to coupling effects. For instance, a ship with 6-DoF at sea subjects to wind and wave loads and is free to sway, this free motion changes the encountered wind speed and therefore the encountering wind pressure and force. So, even with wind tunnel experiment, it is still difficult to evaluate the 'dynamic effects' of a real ship at sea. A vessel's dynamic stability is closely associated with its motion responses, and the motion responses are dependent on both its loading conditions such as displacement, GM, CoG, etc. and external conditions such as the sea state including wind and waves.

Another factor that influences a vessel's motion, and therefore stability at sea, is onboard lifting operation. Vessels such as offshore lifting cranes, wind turbine installation vessels, and fishing vessels that are involved in lifting operations experience complex dynamic motions due to coupling effects from the suspended load (Nojiri and Sasaki, 1983). With a suspended load and an initial heel angle, the restoring moment is asymmetric and is nonlinear.

When this restoring nonlinearity is large enough, mixing frequencies effects can be introduced which is possible to develop roll motion at resonance even with wave excitation frequency far from the roll natural frequency (Bulian and Francescutto, 2011). This complex roll motion in waves is further aggravated by the dynamic lifting load which is not negligible (Jeong et al., 2016). In some cases, the vessel is more prone to be capsized by the combination of the lifting operation and waves (Mantari et al., 2011). The study of the dynamic effects of lifting operation is further elaborated in a separate upcoming paper by the same corresponding author, so its effects are only briefly included in this study.

Previous research basically covered the areas of wind effects, stability in waves, and lifting operation at sea. But they are discussed separately and the combined effects from wind and waves are yet to be further investigated. This study intends to fill this gap and includes wind loads into motion predictions by utilizing URANS solver in commercial software package of STAR-CCM+ to calculate, in full scale, the vessel's motion responses under the combined effects of beam wind, regular beam waves, and lifting operation, by which a vessel's intact stability at sea can be addressed in a holistic manner. To achieve this, a four-step approach is taken:

- URANS-based numerical models of 1:20 and 1:1 are developed and a verification and validation study is performed.
- Scaling effects on roll motion in regular beam waves are examined and quantified.
- The lateral wind is modelled and wind-induced stability loss in calm water is evaluated.
- Finally, the transverse stability of the vessel under the combined effects of lifting, wind and wave is investigated and the correlation between individual factors is studied.

2. COMPUTATIONAL METHOD

2.1 GOVERNING EQUATIONS AND TURBULENCE MODEL

Based on Reynolds decomposition theory (Reynolds, 1895), the continuity and momentum equations for the two-phase immiscible and incompressible flow (water and air) take their forms of Eq. (1) & (2) (Ferziger and Peric, 2020):

$$\frac{\partial(\rho \bar{u}_i)}{\partial x_i} = 0 \quad (1)$$

$$\frac{\partial(\rho \bar{u}_i)}{\partial t} + \frac{\partial}{\partial x_j} (\rho \bar{u}_i \bar{u}_j + \rho \overline{u'_i u'_j}) = -\frac{\partial \bar{P}}{\partial x_i} + \frac{\partial \bar{\tau}_{ij}}{\partial x_j} \quad (2)$$

where

$$\tau_{ij} = \mu \left(\frac{\partial \bar{u}_i}{\partial x_j} + \frac{\partial \bar{u}_j}{\partial x_i} \right) \quad (3)$$

are the mean viscous stress tensor components, \bar{u}_i and \bar{P} are the time-averaged velocity and pressure field in Cartesian coordinates, ρ is fluid (water/air) density, g is gravitational acceleration, and μ is the dynamic viscosity.

The closure of the URANS equations is achieved by introducing the K-Omega turbulence model due to its better performance over the KE model for boundary layers including the viscous-dominated region under adverse pressure gradients (Menter, 1994).

2.2 VESSEL GEOMETRY

Figure 1 shows a numerical model of scale 1:20 of Bluefin (IMO no.: 8000032, Official no.: 386130) which is a fishing training vessel under operation in Australia Maritime College, University of Tasmania. The origin of the coordinate system for Bluefin is located at aftmost (stern) on the baseline level which is the same with the origin of the numerical computational domain. Table 1 lists the main particulars of the model and Table 2 reports the loading conditions from Bluefin stability booklet. The suspended load was integrated into the physical model by increasing the total mass and also applying the equivalent change in the position of the centre of gravity (Lewis, 1988). Later, after validation, the suspended load was modelled with a connecting 'rope' in CFD with the other end fixed at the tip of the lifting boom. The mass in full scale is 3 tonnes which is the same with the rated safe working load of the onboard crane. The position of the suspended load is also the same with that on the real ship.

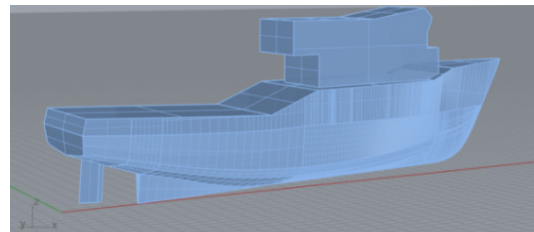


Figure 1. Bluefin numerical model

Table 1. Main particulars of the model (Lab coordinate system)

	Full scale	Model scale
Loa	34.50 (m)	1.725 (m)
Lpp	30.10 (m)	1.505 (m)
B	10.00 (m)	0.500 (m)
D	4.496 (m)	0.225 (m)
Midship	17.30 (m)	0.865 (m)
Rise of Keel	0.74 m over 25.50 m	0.037 m over 1.275 m
Lightship Displacement	413.56 t	50.434 kg
Gross tonnage	387.30 t	47.232 kg
Pos.	(17.3, -6.0, 18.8) m	(0.865, -0.3, 0.94) m

Table 2. Loading conditions (full scale)
(+ve: trim by stern)

	LC5	LC3
Displacement	452.16 t	554.72 t
Draught	3.574 m	3.98 m
LCG	15.91 m	15.62 m
TCG	0.00 m	0.00 m
KG	5.02 m	4.73 m
Trim	+0.03 deg	+0.06 deg
W_{Lift}	3 t	3 t

2.3 FLUID DOMAIN, BOUNDARY CONDITIONS, AND MESH DEVELOPMENT

The computational domain and boundary conditions as shown in Figure 2 are developed according to the guidelines of ITTC (2014).

The hexahedral trimmer is selected to generate volume mesh because of its robustness and high efficiency (Siemens, 2020). Prism layer mesher is also used to capture the viscous effects around the vessel. Three tiers of mesh refinement on free surface are applied with the finest mesh in the vicinity of the overset regions. Within $\pm 5L_{pp}$ of the model, cells numbers are no less than 10 per wave height and are about 180 per wavelength on both port and starboard sides (Siemens, 2020). All y^+ wall treatment is chosen, and a non dimensionalised distance of 100 from the wall (the shell plate of the model) is used as recommended by ITTC (2014). Multi-region overset meshes are employed to simulate the dynamic effects from the suspended load and to capture large motions of the model. Linear interpolation between the donor and acceptor cells is implemented through the ‘hole-cutting’ process during numerical simulation, by which the flow information such as pressure and velocity gradients are transferred between multi-overset regions and the background region. Similar interpolation also takes place at the boundary between the lift region and the vessel region. The mesh set-up is shown in Figure 3.

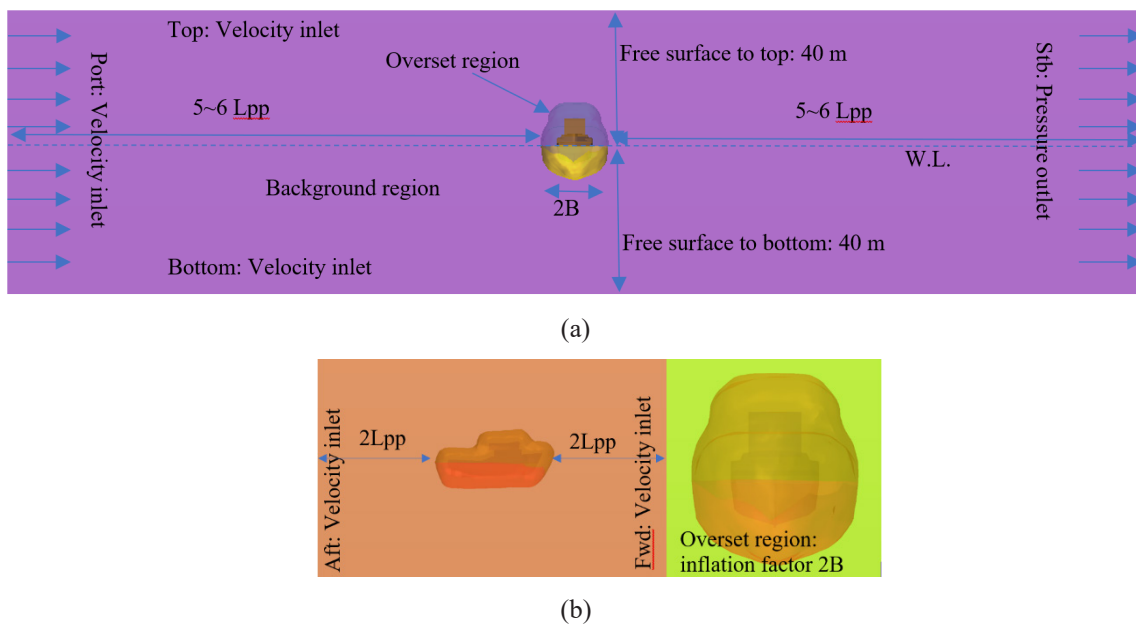
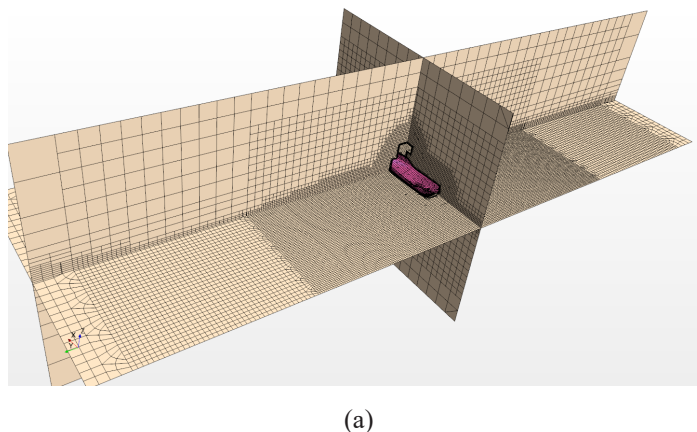


Figure 2. Schematic of the computational domain with boundary conditions, (a) overview of the domain, (b) side and aft view for the overset region



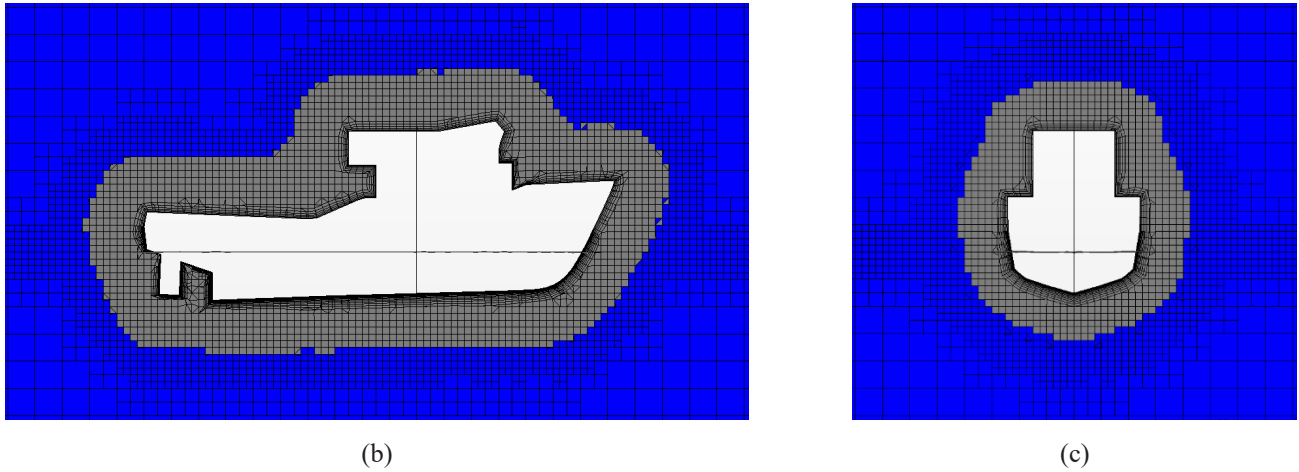


Figure 3. Example of mesh layout, (a) overview of the mesh set-up, (b) side view of the overset region, (c) close-up view for prism layers

2.4 VOLUME OF FLUID METHOD FOR WAVE MODELLING

The Volume of Fluid method is employed for modelling the fifth-order Stokes wave based on the work by Fenton (1985) as it more closely resembles a wave in the real world (Siemens, 2020). The water level is set at 0 m vertically with a depth of -0.8 m. The waves are specified by frequency and height whilst the wavelength is calculated automatically by STAR-CCM+ solver. Wave advancing direction is set from the port side of the model to its starboard side where the suspended load is located 0.3 m to CoG at starboard amidship with a height of about 0.94 m in model scale). The current speed is also set to zero in this study.

2.5 CFD VERIFICATION

2.5.1 Verification for Model-scale Roll Motion in Regular Beam Waves

To evaluate the numerical uncertainties within this simulation set-up, the verification study follows ITTC (2017) guidelines, incorporating the procedure described by Stern et al. (2001). The parameters of interest at this stage are mean roll amplitudes at steady stage and roll centre offset due to the suspended load.

Numerical error (δ_{SN}) in simulation can be decomposed into four contributions: iteration number δ_p , grid size δ_G , time step δ_t , and other parameters δ_p , i.e., given by Eq. (4),

$$U_{SN}^2 = U_I^2 + U_G^2 + U_T^2 + U_P^2 \quad (4)$$

In this study, U_I and U_P are neglected due to an uncertainty magnitude of less than 0.2% in STAR-CCM+ RANS solver (Tezdogan et al., 2015). As a result, simulation numerical uncertainty U_{SN} becomes Eq. (5):

$$U_{SN}^2 = U_G^2 + U_T^2 \quad (5)$$

For the mesh sensitivity study, a sample case in regular beam waves of a height of 0.2 m is selected as using smaller waves can be computationally expensive. The highest frequency of 0.82 Hz is chosen since the roll amplitudes are smaller in high-frequency waves as per EFD result reported in Table 4, and the same amount of discrepancy between each mesh solution (Table 3) on a smaller scale leads to a higher uncertainty rate. Multiple solutions for the mean value of the roll amplitudes with a refinement ratio of about $r_G=1.54$ were taken based on this mesh set-up with the smallest time step (0.001 s) although $r_G=2^{0.5}$ is suggested by ITTC (2017). The ratio of convergence for grid is calculated by Eq. (6) as recommended by (ITTC, 2017):

$$R_G = \frac{\varepsilon_{medium-fine}}{\varepsilon_{coarse-medium}} = \frac{S_3 - S_4}{S_2 - S_3} \quad (6)$$

in which, S represents the solution of a particular grid, i.e., the cells amount for each successive solution S_{N+1} ($N=1\sim5$) is about 1.54 times of the previous one S_N . Notice that the subscripts for solutions are different from ITTC-suggested S_1, S_2, S_3 approach because six solutions were taken for the mesh sensitivity study. Also, the order of the subscript was changed to usual practice – starting from No.1 (coarsest) on the left of the horizontal axis to the right No.6 (finest). The 2nd, 3rd, and the 4th solution were selected for Richardson extrapolation analysis, and monotonic convergence was achieved with an uncertainty rate of about $U_{G, H200} = 7.8\%$.

Table 3. Cells number of each solution and mean roll amplitudes (model scale) at steady stage

Solution no.	Cells number (million)	Mean roll amplitude (deg)
1	0.761	5.47
2	1.229	5.73
3	1.901	5.87
4	2.914	5.92
5	4.487	5.95
6	9.172	6.10

Table 4. Mean roll amplitudes at steady stage for LC5 during model-scale EFD in regular beam waves

No.	Wave height (m)	Wave fre. (Hz)	Mean roll amplitudes (deg)
1	0.2	0.82	6.0
2	0.2	0.38	28.0
3	0.2	0.3	10.5

Solution 5 and 6 can be regarded as two extra steps to examine the sensitivity of this mesh set-up. As from the simulation result, the roll amplitude increases up to 0.2 degrees which is about 3.3% of the selected solution. For this study, 0.2 degrees of roll motion does not make big difference since the focus is transverse stability and a ship at sea that rolls 0.2 degrees more will be insignificant. Considering the computational cost, the 1.9-million mesh (solution 3) with an uncertainty rate of 7.8% was selected as the final mesh.

For time step convergence, the fine mesh (solution 4) is selected as using solution 5 or 6 could be dissipative. Time step refinement ratio is set to 2 with base size calculated by Eq. (7):

$$\Delta t = \frac{CFL * \Delta l}{v_s} \quad (7)$$

and set no larger than 0.4 CFL (Courant-Friedrichs-Lewy) number as recommended by Siemens (2020). Based on the simulation result reported in Figure 4(b), the time step of 0.002 s which is about 0.22 times CFL number yielded a result with an uncertainty rate of $U_{T, H200} = 7.7\%$ is selected.

Figure 4 reports the result of mesh sensitivity study and time step convergence. As per calculation, total numerical uncertainty for solution no.3 is

$$U_{SN_waves} = (U_{G, H200}^2 + U_{T, H200}^2)^{0.5} = (7.8^{0.5} + 7.7^{0.5})^{0.5} = 11\%.$$

This rate is a bit higher but it is obtained from a relatively small scale of roll amplitudes (5.73~5.92 degrees) which has a small denominator – about 6 degrees, meaning that even one degree of difference will trigger roughly 17% uncertainty rate. Besides, it is obtained by using the smallest roll amplitudes (refer to Table 4) which gives the largest error rate. The used frequency of 0.82 Hz is also the highest one that is not likely to encounter at sea. Given that one degree roll motion in the real world will be insignificant to the ship’s roll motion and transverse stability, it is accepted in this study.

Since the mesh for wave height 0.2 m is verified, it should be able to solve larger waves such as $H = 0.25 m$, $H = 0.3 m$ and above because the cells number for the

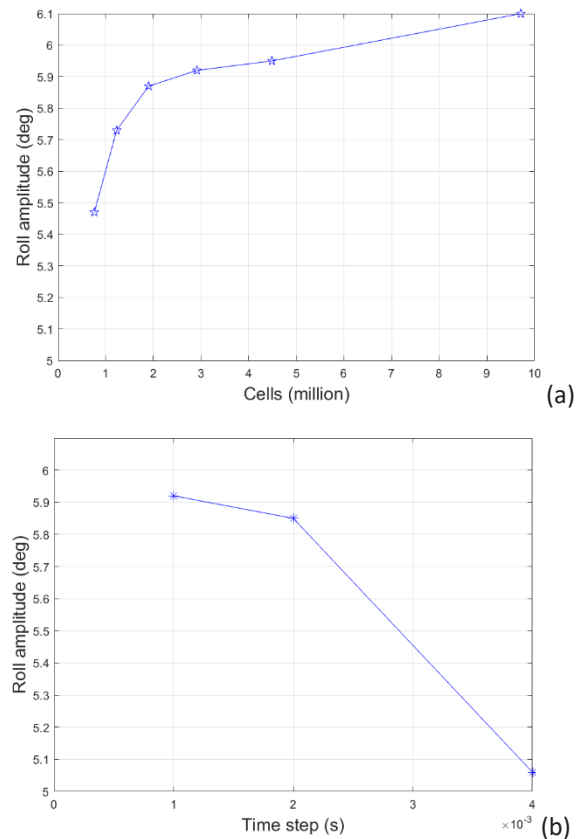


Figure 4. Mesh and time step convergence for roll motion response in model-scale regular beam waves, $H=0.2 m, f=0.82 Hz$, in model scale (a) mean roll amplitudes at steady stage for different mesh solutions (b) mean roll amplitudes for different time steps

smaller waves (in terms of wave height) is fixed, so a higher wave would take more vertical space in the computational domain, resulting in more cells number, i.e., a finer mesh. Therefore using this solution to resolve higher waves should yield a more accurate result. So, verification for higher wave heights is not conducted. Notice that, for this mesh set-up, the number of cells per wave height should remain the same for wave height 0.15 m and 0.10 m (Siemens, 2020). The time step is decided by the flow feature rather than the CFL condition (Anderson, 1995). Therefore, verifications for wave heights of 0.15 m and 0.10 m are not repeated. Instead, by applying the same rule of cells number to the 0.15 m and 0.10 m waves and same set-ups, the selected solution 3 (the 1.9-million one for $H=0.2 m$ waves) yields mesh cells about 3.5 million and 6 million for those two wave heights (0.15m & 0.1 m) and they are selected for validation and further investigation.

2.5.2 Verification for Wind Forces in Full Scale

a) Grid and time step convergence for full-scale wind forces

To verify wind forces, the model is fixed at all six degree of freedom and is adjusted to full scale as full-scale results are more intuitive and straightforward without having to extrapolate from model scale. Wave height is set to zero as well as the current speed. Only area above the main deck (5.1 m above the base line) is included in this calculation for simplification and representative height is used as recommended by ITTC (2021b). Reference wind speed is 25 m/s from port to starboard of the model and Figure 5 illustrates wind direction $\Psi=90$ degrees and representative height in the Cartesian coordinate system.

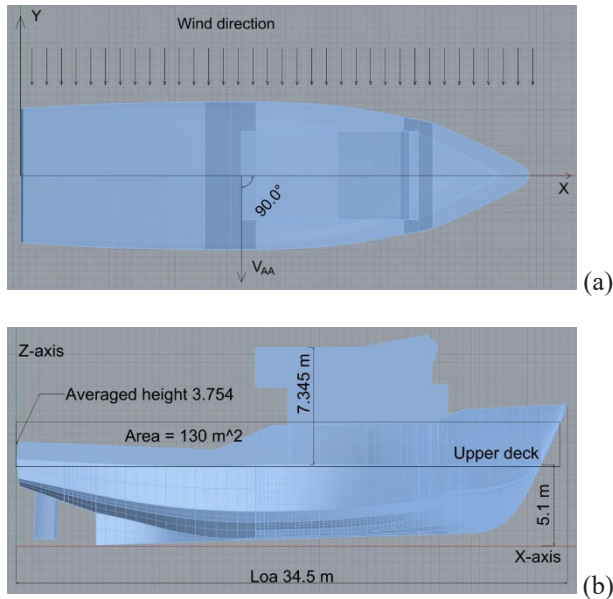


Figure 5. Coordinate system for wind forces calculation in full scale, (a) wind direction, (b) windage area

The refinement ratio for grid convergence is set to $r_G=1.47$ and $r_T=2$ for time step convergence. While grid convergence is performed with the smallest time step, time step convergence is carried out with the finest grid. Figure 6(a) reports an oscillatory convergence of wind force and the uncertainty rate is 4.2%, calculated by Eq. (8) (ITTC, 2017):

$$U_G = \frac{1}{2}(S_{max} - S_{min}) \quad (8)$$

Figure 6(b) shows the result of time step convergence. As per calculation, the uncertainty rate for the time step is about 9% and the total uncertainty rate for wind force is

$$U_{SN_wind} = \sqrt{U_G^2_{wind} + U_T^2_{wind}} = \sqrt{4.2^2 + 9^2} = 10\%$$

To be in line with those for waves, the finer mesh and the smaller time step are chosen.

b) Wind force verification

Having verified the mesh set-up, the aerodynamic forces are calculated for five wind nominal speeds (10, 15, 20, 25,

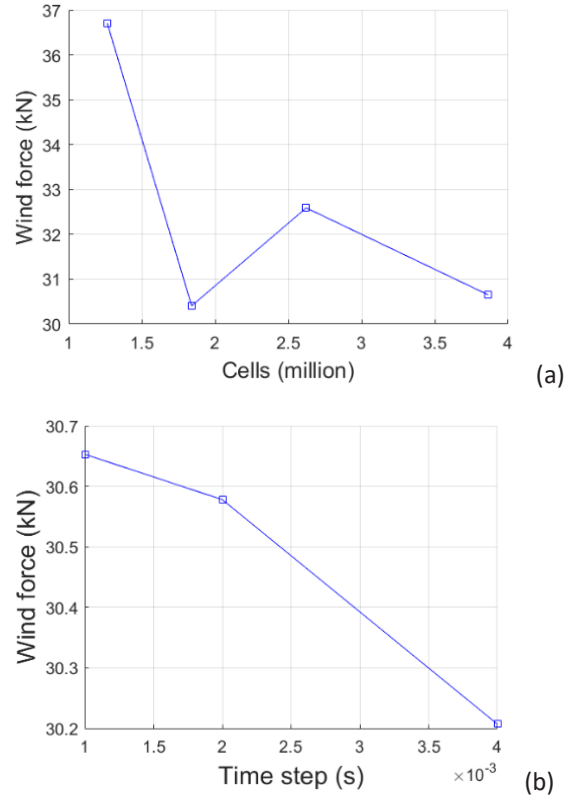


Figure 6. Full-scale grid and time step verification for wind force, LC5, wind direction: lateral, speed: 25 m/s

and 30 m/s) with wind direction of $\psi = 90$ degrees in full scale and compared with static analytical calculation in accordance with guidelines from ITTC (2021b) by Eq. (9):

$$C_{DAY}(\psi) = \frac{R_{AAY}(\psi)}{q_A \cdot A_{XZ}} \quad (9)$$

Where C_{DAY} denotes the aerodynamic force coefficient at transverse (Y) direction ($\Psi = 90$ deg), R_{AAY} is the aerodynamic force at transverse (Y) direction, and A_{XZ} represents side windage (lateral projected) area. The dynamic air pressure q_A at low Mach number is considered constant for a given speed and expressed as Eq. (10):

$$q_A = \frac{1}{2} \cdot \rho_A \cdot V_{AY}^2 \quad (10)$$

in which ρ_A is air density and V_{AY} is height-averaged wind velocity at Y (transverse) direction and is given by Eq. (11)

$$V_{AY}^2 = \frac{1}{H_L} \int_0^{H_L} V(z)^2 dz \quad (11)$$

where H_L is mean height in lateral plane and V_z is height averaged wind speed while z is height at each equally spaced interval between 0 and H_L .

Figure 7(a) reports the difference of wind forces between CFD results and analytical calculation which is about 11~15% and Figure 7(b) shows the result of wind force coefficients which are obtained by substituting Eq (11) into Eq (10). Then using Eq (9) and obtained wind force from full-scale CFD simulations as reported in Figure 7(a).

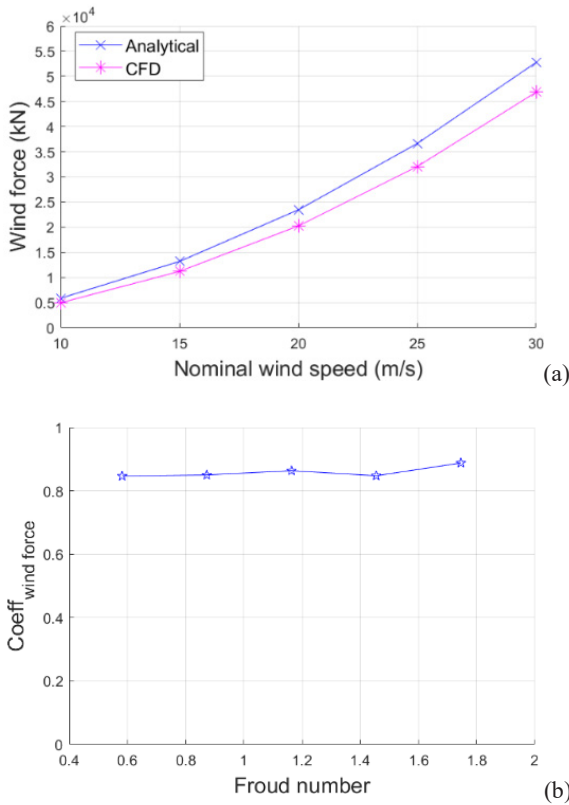


Figure 7. Full-scale wind force verification, LC5, (a) wind force difference between CFD and analytical calculation, (b) wind force coefficients for different Froude number

2.6 MODEL-SCALE CFD VALIDATION FOR MOTION RESPONSE IN REGULAR BEAM WAVES

The experimental test was carried out in the AMC (Australia Maritime College, University of Tasmania) model test basin and a 1:20 scale model of Bluefin was used. The suspended load was integrated into the model by adding additional mass and spreading them to obtain the correct position of the gravity centre. Two loading conditions were considered each of which consists of four wave heights 0.05, 0.1, 0.15, and 0.2 m with a range of frequencies as detailed in Table 5.

Table 5. Wave and loading conditions tested (model scale)

Loading condition	Wave type	Wave H (m)	Wave f (Hz)
LC5/LC3	regular beam	0.05	0.30
LC5/LC3	regular beam	0.05	0.38

LC5/LC3	regular beam	0.05	0.53
LC5/LC3	regular beam	0.05	1.02
LC5/LC3	regular beam	0.05	1.44
LC5/LC3	regular beam	0.10	0.3
LC5/LC3	regular beam	0.10	0.38
LC5/LC3	regular beam	0.10	1.02
LC5/LC3	regular beam	0.15	0.3
LC5/LC3	regular beam	0.15	0.38
LC5/LC3	regular beam	0.15	1.02
LC5/LC3	regular beam	0.20	0.3
LC5/LC3	regular beam	0.20	0.38
LC5/LC3	regular beam	0.20	0.82

Using the transfer function, the roll amplitudes are nondimensionalised by dividing max wave slope (Molland, 2008), i.e.,

$$RAO_{roll} = \frac{roll\ amplitude\ \varphi\ (rad)}{max\ wave\ slope\ \vartheta\ (rad)} \quad (12)$$

where max wave slope is

$$\vartheta = 0.5H_w \cdot k = \frac{0.5H_w \cdot 2\pi}{L_w} (rad) \quad (13)$$

The calculated RAOs from EFD and CFD are compared, and reasonable agreement is achieved as reported in Figure 8. A further step was taken, and the RAO is calculated in Maxsurf based on strip theory (the green dotted line in Figure 8). It should be mentioned that due to the limitation of the software (Maxsurf motion) used, there is no option to change the transverse position of the gravity centre caused by the suspended load, so the suspended load is not included in the calculation. Therefore the phase shifts are expected because the suspended load changes the roll natural period of each loading condition. Initial thinking was to compare RAO from EFD, CFD and Strip theory for the condition with the suspended load, but since it is not available by Strip method, roll RAO of no-lifting condition by Strip method is used in this comparison considering about the influence by the 3 tonnes suspended load on roll RAO is relatively small and the comparison would roughly give a ballpark range of the values.

It should be mentioned that due to the limitation of testing facilities, wind effects were not modelled during the physical experimental test. So, for the wind force, the CFD model is not validated against EFD, only motion response in waves is validated. However, the convergence of grid and time step for wind force in full-scale CFD is conducted as described in section 2.5.2 (a). Besides, the wind forces with the full-scale model fixed in calm water are calculated

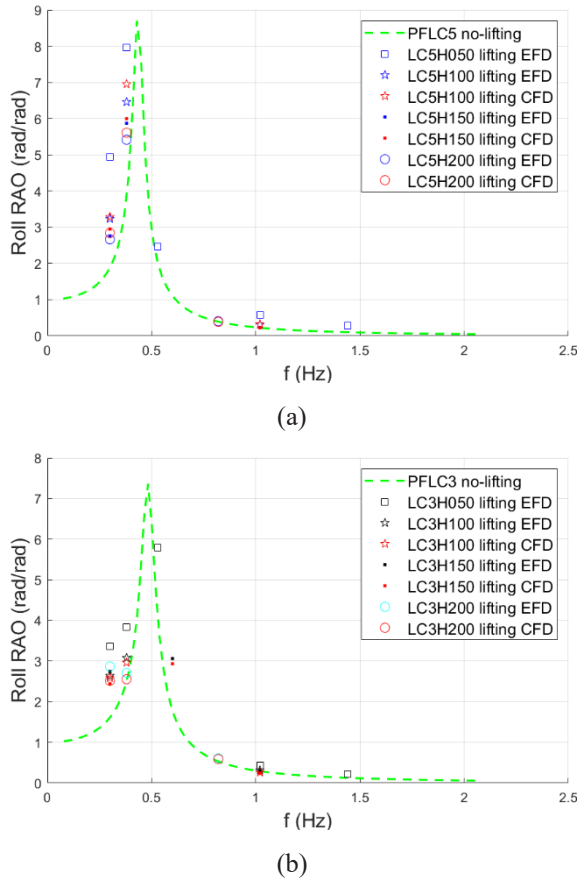


Figure 8. Comparison of roll responses in model scale, PF vs. EFD vs. CFD, (a) LC5, (b) LC3

and compared against the results from analytical calculation and reasonable agreement were observed.

3. RESULTS AND DISCUSSION

3.1 SCALE EFFECTS FOR MOTION RESPONSE IN REGULAR BEAM WAVES

CFD simulations (*LC5*) for both model scale (1:20) and full scale are conducted in regular beam waves with the suspended load of about $0.66\%D$ at the tip of the lifting boom. The model is set to 4-*DoF* (roll, pitch, heave, and sway) in all cases while the suspended load was connected by a numerical ‘rope’ that allows the suspended load to swing freely at all 6-*DoF*. The motions of the suspended load are mostly swing transversely with slightly surge (longitudinal) and rotational motions as well as occasionally jump up and down, but in all cases, it is connected by the ‘rope’ with certain stiffness that makes is equivalent as a rope in the real word. For full-scale simulations, all set-ups are similar with model scale except that all length dimensions are scaled up by 20 times such as the length and width of the model, as well as CFD model mesh size. Displacement related quantities are scaled to 20^3 including the suspended load. The nondimensionalised wall distance of y^+ value is maintained similar to that in model scale.

According to Figure 9(a), At wave frequencies of 0.3, 0.38, & 0.53 Hz (model scale), roll amplitudes are overestimated in model scale by 2.8%, 6.2%, & 9.8% while they are underestimated by 12.1% & 15.0% for higher wave frequencies of 0.82 & 1.02 Hz, respectively. Near the roll natural frequency, as reported in Figure 9(b), roll amplitudes are about 6~7% larger in model scale for all wave heights. Although higher wave frequency gives a shorter wavelength, corresponding to a low Reynolds number and hence a relatively larger proportion of frictional force, it is still difficult to conclude that roll amplitudes are overestimated/underestimated in model scale because most of the values are within CFD uncertainty level (11%), and they appear to be wave-frequency-dependent. Nevertheless, based on current findings, scaling effects account for about 3~15% in terms of roll amplitude depending on wave excitation frequency and about 6~7% near roll resonance frequency for all wave heights

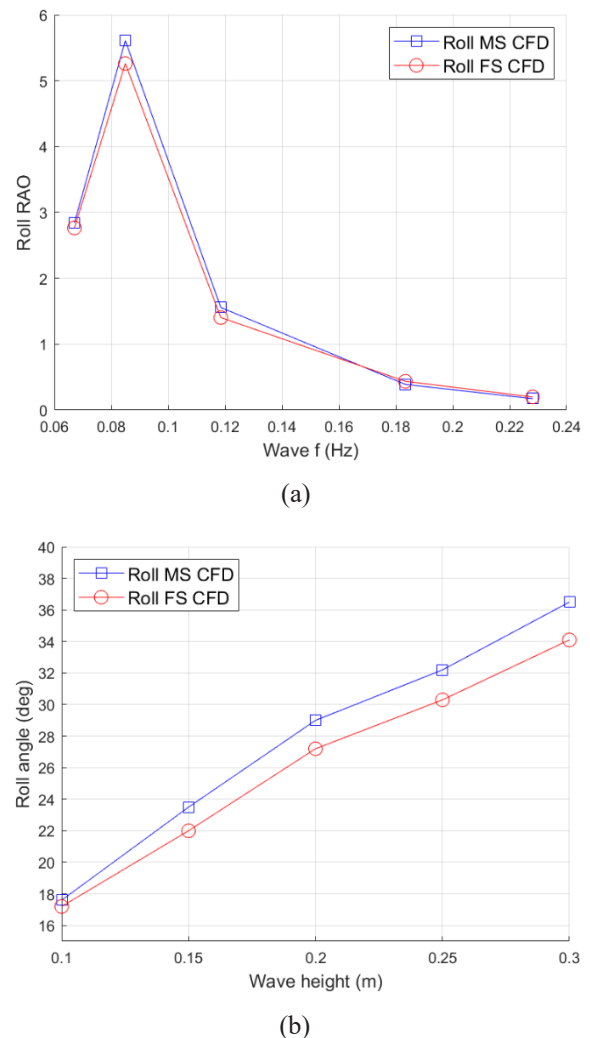
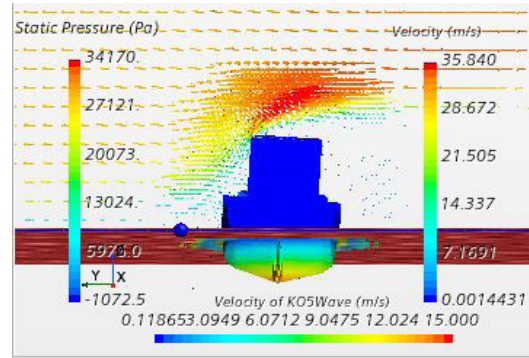


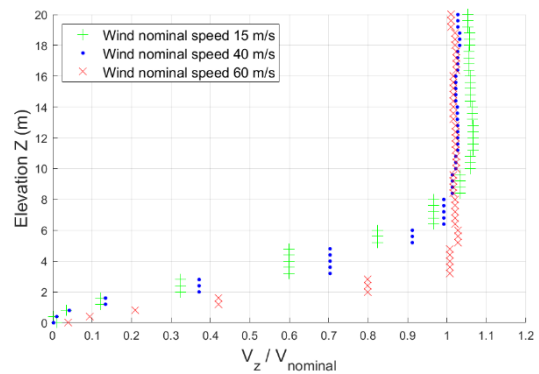
Figure 9. Comparison of mean roll amplitudes in regular beam waves between model scale and full scale, (a) roll RAO at different wave frequencies at wave height 4 m in full scale, (b) mean roll amplitudes at different wave heights for wave frequency 0.085 Hz in full scale

3.2 FULL-SCALE WIND-INDUCED STABILITY LOSS IN CALM WATER

This series of tests consist of eight different wind nominal speeds and the full-scale model is set with 4-DoF in calm water without the suspended load. Figure 10(a) reports the heel angles imposed by the wind at the steady stage when the model inclines to one side and eventually stay at that position with slightly oscillation, corresponding to different extents of stability loss depicted in Figure 10(b). According to Figure 10(a), the winds of different speeds heel the vessel to certain angles disproportionately. Within the normal operational range, the influence of wind is relatively small. Even in a storm (24.5 – 28.4 m/s), the wind alone can only heel the vessel up to about 3 degrees (at steady state) with a maximum of 8 degrees at the beginning. In a very rare and extreme situation such as a violent storm or hurricane (>32.6 m/s), the maximum heel angle by the wind is less than 6 degrees. The other two speeds of 50 & 60 m/s are for theoretical analysis only. An alternative approach of analytical calculation for wind heeling levers per the 2008 IS CODE is also presented in Figure 10(b) as constant wind levers. While Figure 10(c) illustrates one of the simulations of wind-heeling in calm water in full-scale CFD, Figure 10(d) shows that the wind velocity profiles follow a similar pattern.

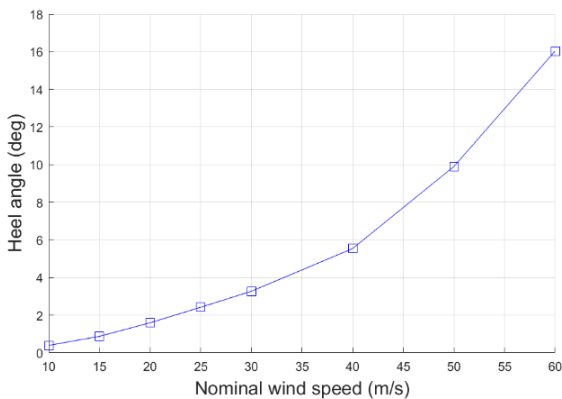


(c)

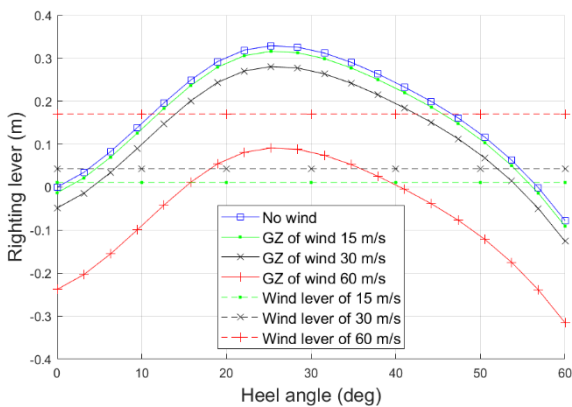


(d)

Figure 10. Full-scale calculation of transverse stability in calm water with lateral wind, (a) wind-induced heel angles, (b) wind-induced stability loss in calm water, (c) example of full-scale wind heeling simulation, (d) wind velocity profiles



(a)



(b)

3.3 FULL-SCALE TRANSVERSE STABILITY UNDER LIFTING CONDITIONS IN WIND AND WAVES

This series of numerical simulations are carried out with the 6-DoF suspended load connected by a numerical ‘rope’. Wind and waves are modelled to study the correlation between them and the transverse stability. It can be seen from Figure. 11 that the extent of influence from the same wind varies with wave frequency and wave height.

In Figure. 11(a), near the roll natural frequency, the wind has limited amount of influence (about 9%) in terms of roll motion, but at the lowest and highest wave frequencies, roll amplitudes are increased by about 53% and 20% by the wind. It appears that near roll resonance frequency, the wave dominates the motion and hence the wind’s influence is relatively smaller, while at low frequencies waves, the vessel rolls slowly so the wind has sufficient time to act on the vessel during one cycle of roll motion and the vessel obtained more energy from the wind and therefore a bigger influence is expected.

In Figure. 11(b), five wave heights are tested all of which has the same wave frequency (0.085 Hz) which is close

to roll natural frequency. For seakeeping, this frequency is normally of interest since larger roll amplitude can be expected due to roll resonance. As from the CFD result, roll amplitudes are increased by the same wind disproportionately by 2~12% depending on waves heights.

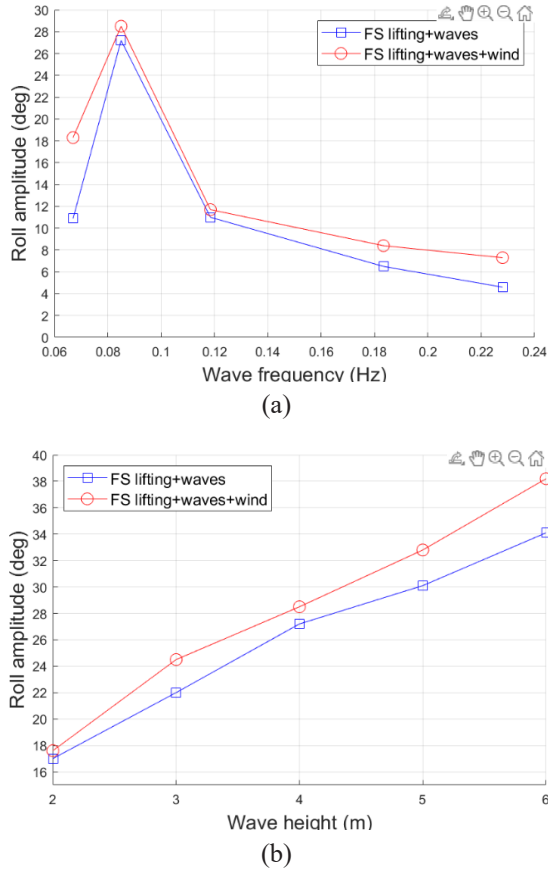


Figure 11. Comparison of mean roll amplitudes with or without wind in full-scale regular beam waves, test condition: LC5, wind speed: 25 m/s, (a) at fixed wave height of 4 m but varying wave frequency, (b) at fixed wave frequency of 0.085 Hz but varying wave height.

A further look into the influence of the same wind at a higher wave height of 6 metres is illustrated in Figure. 12. As per calculation result, influence from the same wind peaks at the lowest wave frequency which is about 22% and the least influence is observed near roll natural frequency which is less than 3%.

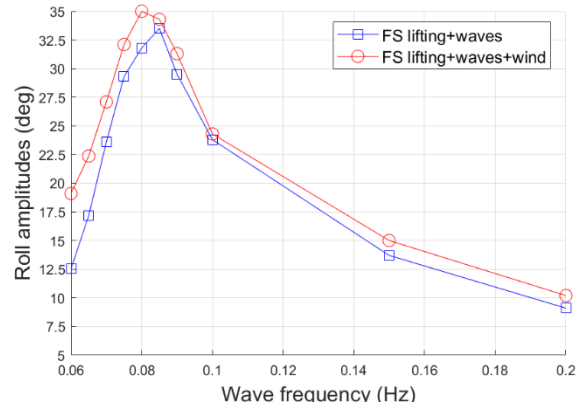


Figure 12. Mean roll amplitudes variation with wind (25 m/s) in different frequencies of full-scale regular beam waves, wave height 6 m

Table 6 reports the tested conditions and Figure. 13 illustrates one of the full-scale simulations in 6-metre wave height near roll natural frequency. It can be seen that the vessel regularly heaves up and down while swaying further to one side. Roll amplitudes at steady stage reach 35 degrees showing a regular sinusoidal pattern with insignificant pitch motion. Surge and yaw are fixed in this study. Wind velocity is represented by small arrows with colours representing the magnitudes. The connecting forces between the vessel and the suspended load are also plotted and a regular pattern is observed at steady stage.

Table 6. Summary of test conditions for stability in full-scale wind and waves for loading condition 5

Simulation no.	Suspended load	Wind speed (m/s)	Wave Hgt. (m)	Wave fre. (Hz)	Heel/ mean roll amplitude (deg)	Wind heel lever (10 ⁻³ m)	Remarks
1	No	10	0	-	0.4	5	static heel
2	No	15	0	-	0.9	11	static heel
3	No	20	0	-	1.6	19	static heel
4	No	25	0	-	2.4	30	static heel
5	No	30	0	-	3.3	43	static heel
6	No	40	0	-	5.5	76	static heel
7	No	50	0	-	9.9	119	static heel
8	No	60	0	-	16.0	171	static heel
9	Yes	25	4	0.067	18.3	-	dynamic
10	Yes	25	4	0.085	28.5	-	dynamic
11	Yes	25	4	0.119	11.7	-	dynamic

12	Yes	25	4	0.183	8.4	-	dynamic
13	Yes	25	4	0.228	7.3	-	dynamic
14	Yes	0	4	0.067	10.9	-	dynamic
15	Yes	0	4	0.085	27.2	-	dynamic
16	Yes	0	4	0.119	11.0	-	dynamic
17	Yes	0	4	0.183	6.5	-	dynamic
18	Yes	0	4	0.228	4.6	-	dynamic
19	Yes	25	2	0.085	17.6	-	dynamic
20	Yes	25	3	0.085	24.5	-	dynamic
21	Yes	25	4	0.085	28.5	-	dynamic
22	Yes	25	5	0.085	32.8	-	dynamic
23	Yes	25	6	0.085	38.2	-	dynamic
24	Yes	0	2	0.085	17.0	-	dynamic
25	Yes	0	3	0.085	22.0	-	dynamic
26	Yes	0	4	0.085	27.2	-	dynamic
27	Yes	0	5	0.085	30.1	-	dynamic
28	Yes	0	6	0.085	34.1	-	dynamic
29	Yes	25	6	0.060	19.1	-	dynamic
30	Yes	25	6	0.065	22.4	-	dynamic
31	Yes	25	6	0.070	27.1	-	dynamic
32	Yes	25	6	0.075	32.1	-	dynamic
33	Yes	25	6	0.080	35.0	-	dynamic
34	Yes	25	6	0.085	34.3	-	dynamic
35	Yes	25	6	0.090	31.3	-	dynamic
36	Yes	0	6	0.060	12.6	-	dynamic
37	Yes	0	6	0.065	17.2	-	dynamic
38	Yes	0	6	0.070	23.6	-	dynamic
39	Yes	0	6	0.075	29.3	-	dynamic
40	Yes	0	6	0.080	31.8	-	dynamic
41	Yes	0	6	0.085	33.5	-	dynamic
42	Yes	0	6	0.090	29.5	-	dynamic

4. CONCLUDING REMARKS

URANS-based model-scale and full-scale simulations are conducted and the modelling approach has been verified. Transverse stability under lifting condition is investigated in both calm water and in regular beam waves. Scaling effects are examined and upon verifying wind resistance, the combined influence from the suspended load, the wind, and the waves is evaluated in full-scale *CFD* simulations. The findings are summarised as follows:

- Scale effects account for about 3~15% in terms of roll amplitudes and it appears to be both frictional-force related, and wave-frequency dependent. But near the roll natural frequency, roll amplitudes are overestimated for all wave heights by about 6~7%.
- Wind force has different extent of influence on the vessel's transverse stability, and wind velocity profile near the vessel follows a certain predictable pattern.

In calm water, a wind of 30 *m/s* in full scale heels the vessel to about 3.3 degrees which are close to the heel angle (3.2 *deg*) by a 0.66%*D* suspended load.

- The correlation between roll motion and combined effects of wind, waves and the suspended load is complicated and further investigation is needed. However, wave excitation frequency seems to affect the extent of influence from the wind on the roll motion. Maximum increase of about 53% is observed at the lowest frequency, about 20% at the highest frequency, and about 2~12% near the roll natural frequency.

5. ACKNOWLEDGEMENTS

The authors appreciate the strong support from HPC resources funded by Australia Maritime College, University of Tasmania for cloud computation. A big thanks also goes to Siemens support team who provides excellent technical support in *CFD* modelling.

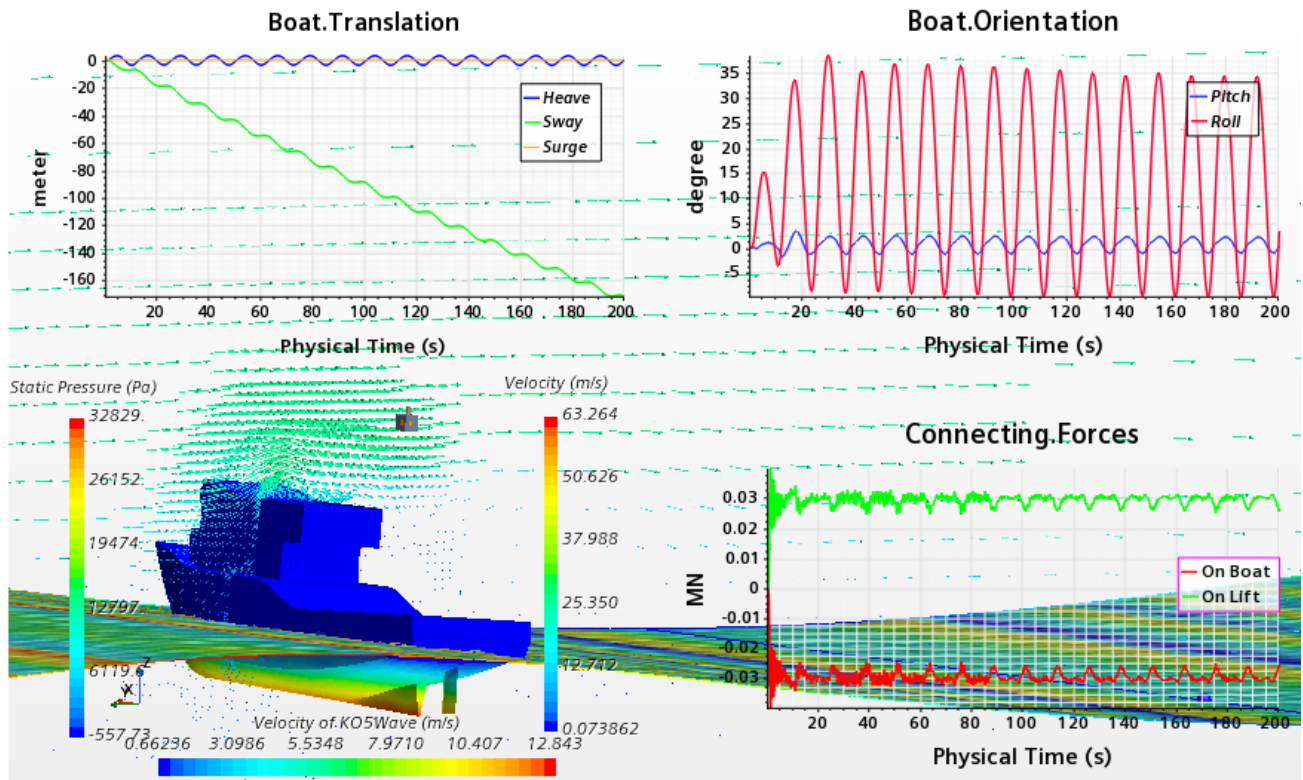


Figure 13. Full-scale simulation of lifting operation in wind and waves, LC5, wind speed: 25 m/s, waves: $H = 6$ m, $f = 0.085$ Hz, (a) upper left, heave and sway motions of the model, (b) upper right, roll and pitch motion of the model, (c) lower left, pressure distribution and wind/water visualisation, (d) lower right, connecting forces between the model and the suspended load

6. REFERENCES

1. ANDERSEN, I. M. V. 2013. *Wind loads on post-panamax container ship*. Ocean Engineering, Vol. 58, 19.
2. ANDERSON, J. D. 1995. *Computational fluid dynamics*, USA, McGraw-Hill.
3. BULIAN, G. & FRANCESCUTTO, A. 2011. *Effect of roll modelling in beam waves under multi-frequency excitation*. Ocean Engineering, 38, 1448-1463.
4. DEAKIN, B. & WRIGHT, M. A. 2005. *Wind heeling moment on multihull vessels*. International Conference on Fast Sea Transportation. St. Petersburg, Russia.
5. FENTON, J. D. 1985. *A fifth-order Stokes theory for steady waves*. Journal of Waterway, Port, and Ocean Engineering, III, 19.
6. FERZIGER, J. H. & PERIC, M. 2020. *Computational Methods For Fluid Dynamics*, Berlin, Germany, Springer.
7. IMO 1985. *WEATHER CRITERION*. Resolution A.562(14).
8. IMO 1993. *CODE ON INTACT STABILITY FOR ALL TYPES OF SHIPS COVERED BY IMO INSTRUMENTS*. Resolution A.749(18).
9. IMO 2008. *Adoption of the international code on intact stability, 2008 (the 2008 IS CODE)*. Maritime Safety Committee, Resolution MSC.267(85).
10. ITTC 2014. *Practical Guidelines for Ship CFD Applications*. ITTC - Recommended Procedures and Guidelines, 7.5-03-02-03, 19.
11. ITTC 2017. *Uncertainty Analysis in CFD Verification and Validation Methodology and Procedures*. ITTC - Recommended Procedures and Guidelines, 7.5-03-01-01, 13.
12. ITTC 2021a. *Estimation of Roll Damping*. ITTC Quality System Manual, 7.5-02-07-04.5, 47.
13. ITTC 2021b. *Guideline on the CFD-based Determination of Wind Resistance Coefficients*. ITTC Quality System Manual Recommended Procedures and Guidelines, 7.5-03-02-05, 7.
14. JANSSEN, W. D., BLOCKEN, B. & VAN WIJHE, H. J. 2017. *CFD simulations of wind loads on a container ship: Validation and impact of geometrical simplifications*. Journal of Wind Engineering and Industrial Aerodynamics, 166, 106-116.
15. JEONG, D.-H., ROH, M.-I. & HAM, S.-H. 2016. *Lifting simulation of an offshore supply vessel considering various operating conditions*. Advances in Mechanical Engineering, 8.

16. JIN, Y., CHAI, S., DUFFY, J. & CHIN, C. *Scale Effects on Hydrodynamic Manoeuvring Force Prediction*. Proceedings of the Twenty-fifth (2015) International Ocean and Polar Engineering Conference, June 21-26, 2015 Kona, Big Island, Hawaii, USA. ISOPE, 6.
17. KOK, Z., DUFFY, J., CHAI, S., JIN, Y. & JAVANMARDI, M. 2020. *Numerical investigation of scale effect in self-propelled container ship squat*. Applied Ocean Research, 99.
18. LEWIS, E. V. 1988. *Principles of Naval Architecture Second Revision*, 601 Pavonia Avenue Jersey City, NJ, The Society of Naval Architects and Marine Engineers.
19. MANTARI, J. L., SILVA, R. C. & SOARES, C. G. 2011. *Intact stability of fishing vessels under combined action of fishing gear, beam waves and wind*. Ocean Engineering, 38, 1989-1999.
20. MENTER, F. R. 1994. *Two-equation eddy-viscosity turbulence models for engineering applications*. AIAA Journal, 32, 1598-1605.
21. MOLLAND, F. A. 2008. *The maritime engineering reference book*, Budapest, Hungary. Macmillan.
22. NOJIRI, N. & SASAKI, T. 1983. *Motion Characteristics of Crane Vessels in Lifting Operation*. Offshore Technology Conference. Houston, Texas, USA.
23. OH, K. J. & KANG, S. H. 1992. *Full scale Reynolds number effects for the viscous flow around the ship stern*. Comput. Mecha., 9, 10.
24. REYNOLDS, O. 1895. *On the Dynamical Theory of Incompressible Viscous Fluids and the Determination of the Criterion*. Philosophical Transactions of the Royal Society of London, A.186, 41.
25. SAYDAM, A. Z. & TAYLAN, M. 2018. *Evaluation of wind loads on ships by CFD analysis*. Ocean Engineering, 158, 54-63.
26. SIEMENS 2020. *STAR CCM+ User Guide*. Siemens technical file, 15.04. Munich, Germany
27. SPYROU, K. J. 2011. *A Basis for Developing a Rational Alternative to the Weather Criterion: Problems and Capabilities*. In: NEVES, M. A. S., BELENKY, V. L., KAT, D. J. O., SPYROU, K. J. & UMENDA, N. (eds.) *Contemporary Ideas on Ship Stability and Capsizing in Waves*. Springer. New York, NY.
28. STERN, F., WILSON, R. V., COLEMAN, H. W. & PATERSON, E. G. 2001. *Comprehensive Approach to Verification and Validation of CFD Simulations—Part 1: Methodology and Procedures*. Journal of Fluids Engineering, 123, 793-802.
29. TEZDOGAN, T., DEMIREL, Y. K., KELLETT, P., KHORASANCHI, M., INCECIK, A. & TURAN, O. 2015. *Full-scale unsteady RANS CFD simulations of ship behaviour and performance in head seas due to slow steaming*. Ocean Engineering, 97, 186-206.
30. VASSALOS, D., JASIONOWSKI, A. & CHCHOWICZ, J. 2003. *Weather criterion - questions and answers*. International Conference on the Stability of Ships and Ocean Vehicles. Madrid, Spain: International Ship Stability Workshop.